

# Effects of land cover type and greenness on advanced very high resolution radiometer bidirectional reflectances: Analysis and removal

Aisheng Wu,<sup>1,2</sup> Zhanqing Li, and Josef Cihlar

Canada Centre for Remote Sensing, Ottawa, Ontario, Canada

**Abstract.** The objectives of the study are (1) to examine the effects of land cover type, green biomass, and solar zenith angle (SZA) on the bidirectional reflectance distributions (BRDs) of the visible and near-infrared advanced very high resolution radiometer (AVHRR) data from NOAA 11 over terrestrial surfaces; and (2) to correct for these effects by developing BRD functions (BRDF). Four land cover types are examined: barren, grassland, forest, and cropland. The data used consist of 1-km daily AVHRR measurements for three growing seasons collected over 19 homogeneous land sites ( $20 \times 20 \text{ km}^2$  for each site) in the conterminous United States and parts of Canada. BRD is found to be strongly land cover dependent. For the same cover type, BRD is altered significantly by the green biomass present (represented by the normalized difference vegetation index (NDVI)). The effects of SZA on BRDs are also observed over all surface types under investigation. Semiempirical BRDFs were developed to account for these effects that are the functions of the SZA, satellite viewing zenith angle, relative azimuth angle, and NDVI. Good agreements were found between the observed and the modeled bidirectional dependencies for wide ranges of NDVI and SZA. A single BRDF appears to be sufficient for bidirectional correction of the clear-sky AVHRR measurements made over a specific land cover type throughout a season. Finally, the developed BRDFs were used to normalize AVHRR reflectance data to a common geometry and to infer the hemispherical albedos for monitoring the seasonal variations of land surfaces.

## 1. Introduction

The advanced very high resolution radiometer (AVHRR) on board the NOAA polar orbiting satellites has provided continuous global measurements at a fairly high resolution for more than a decade. Therefore AVHRR archives have served as an important data source for monitoring the changes of the Earth's environment, in addition to the primary application in facilitating day-to-day weather forecasting. AVHRR channels 1 and 2 measure the visible (0.58–0.68  $\mu\text{m}$ ) and near-infrared (0.72–1.10  $\mu\text{m}$ ) reflected radiances, respectively. They are often used for remote sensing of the terrestrial surfaces. However, these measurements are affected significantly by Sun-target-sensor geometry because most types of natural surfaces are anisotropic reflectors [Kriebel, 1978; Kimes *et al.*, 1984; Kimes and Sellers, 1985; Middleton, 1991]. The AVHRR radiometers scan  $\pm 56^\circ$  relative to the nadir in a plane normal to the satellite track. As a result, a fixed target may be viewed from very different viewing angles, leading to varying reflected radiance. This affects the detectability of the temporal evolution of a target [Gutman, 1991]. The bidirectional depen-

dency also poses problems in the retrieval of surface parameters such as albedo [Li and Garand, 1994] and radiant fluxes [Li and Leighton, 1993], as they are defined over all directions. Therefore bidirectional correction is required for the AVHRR data to be used for both monitoring and retrieving purposes.

Top-of-atmosphere (TOA) bidirectional reflectance distribution functions (BRDFs) over land surfaces have been obtained following two different approaches. One is the theoretical approach which incorporates a surface BRDF into an atmospheric radiative transfer model to simulate the BRDF at the TOA [Gerstl and Simmer, 1986; Lee and Kaufman, 1986; Liang and Strahler, 1993]. In this scheme, surface BRDFs were obtained empirically [e.g., Walthall *et al.*, 1985; Shibayama and Wiegand, 1985], semiempirically [e.g., Roujean *et al.*, 1992a; Rahman *et al.*, 1993], physically [e.g., Hapke, 1981; Kimes, 1984; Verhoef, 1984; Pinty *et al.*, 1989; Verstraete *et al.*, 1990; Gao, 1993], or geometrically [Li and Strahler, 1986; Ross and Marshak, 1988; Strahler and Jupp, 1990]. This approach has two major advantages. First, it allows specification of the spectral bands of any radiometer such as AVHRR [Paltridge and Mitchell, 1990; Mitchell and O'Brien, 1993]. Second, it can provide an insight on how the TOA BRD is modified by the atmosphere, canopy, and underlying surface. However, the theoretical simulations may not represent the conditions that actually exist, owing to the diversity of surface types and topography.

Alternatively, TOA BRDFs were also derived directly from satellite measurements. Taylor and Stowe [1984], for

<sup>1</sup>On sabbatical from the Chinese Academy of Sciences, Institute of Plateau Atmospheric Physics, Lanzhou, China.

<sup>2</sup>Now at the Department of Soil Sciences, University of British Columbia, Vancouver, Canada.

Copyright 1995 by the American Geophysical Union.

Paper number 95JD00512.  
0148-0227/95/95JD-00512\$05.00

example, established broadband BRD models for land, ocean, and clouds using data from the Nimbus 7 Earth Radiation Budget (ERB) radiometers. The ERB data were also employed to construct a more complete set of broadband BRDFs for use in the Earth Radiation Budget Experiment (ERBE) [Suttles *et al.*, 1988]. Because of the lack of a complete set of BRDFs for the individual AVHRR channels, Gutman *et al.* [1989] employed the broadband BRDFs from ERBE to convert AVHRR reflectance (observed from a specific direction) into albedo (defined over the upper hemisphere). The substitution may alleviate the effect of BRD on the derived albedo, but the effect is unlikely to be eliminated completely, as the BRD depends on the wavelength as well as the spatial scale [Pinty and Verstraete, 1992]. The spectral band and field of view (FOV) of both ERB and ERBE are considerably larger than those of AVHRR. This study is confined to the narrowband AVHRR data. A discussion of recent developments in broadband BRDFs can be found elsewhere (Z. Li, submitted to the *Journal of Theoretical and Applied Climatology*, On the angular correction of satellite radiation measurements: The performance of ERBE angular dependence model in the Arctic, 1995). Generally speaking, the finer the spatial resolution the more complex the BRD and more detailed classification of surface type is needed. Therefore the two BRDFs used by ERBE over land, including vegetation and desert, are not sufficient for the bidirectional correction of AVHRR data.

In view of these limitations, direct use of AVHRR measurements was made to study the BRD and to develop the BRDF for clear-sky AVHRR data [Gutman, 1994; Cihlar *et al.*, 1994]. Cihlar *et al.* [1994] analyzed the AVHRR BRD effects for cropland, deciduous and coniferous forest, and wetland in central Canada. Since their study employed the AVHRR data of only 20 days during peak green period, temporal evolution of the BRD was not examined. To account for the dependencies of BRD on land cover type and season, Gutman [1994] developed a BRDF for each month over some selected  $1^\circ \times 1^\circ$  target areas. While this method allows for the diversity of surface type, topography, and seasonal variation, this approach has the disadvantage of using too many basic functions, which may lead to instability in the coefficients developed.

This study follows a similar approach to that of Cihlar *et al.* [1994] but focuses on the effects of seasonality on AVHRR BRD for different surface types. For a given land cover type, the temporal variation of a BRD is driven by two factors, Sun position and physiological condition of the (mostly vegetated) land target. Sun position is determined by azimuth angle and solar zenith angle (SZA). Because of the inherent characteristics of the AVHRR geometry at northern latitudes in summer the dependency on azimuth angle cannot be addressed here. The most revealing indicator of the growing status of a vegetation target is greenness that can be directly observed from space using, for example, the normalized difference vegetation index (NDVI). NDVI depends much more weakly on viewing geometry than visible and near-infrared reflectance [Kimes *et al.*, 1984; Holben *et al.*, 1986; Cihlar *et al.*, 1994]. Therefore this study examines the dependencies of the AVHRR BRD on NDVI and SZA and develops a new set of BRDFs to account for these dependencies. The utility of the BRDFs in land monitoring is also investigated.

**Table 1.** Site Location and Characterization

Site Number	Upper Left Corner		Land Characterization
	Latitude°N	Longitude°W	
1	47.270	117.340	grassland
2	37.570	111.670	grassland
3	40.960	104.840	grassland
4	40.650	99.610	grassland
5	46.830	103.720	grassland
6	48.940	113.325	grassland
7	50.409	111.494	grassland
8	44.750	110.220	forest
9	44.300	103.710	forest
10	48.855	114.393	forest
11	47.614	72.080	forest
12	51.728	101.800	forest
13	42.533	72.333	forest
14	41.490	101.090	cropland
15	41.370	95.690	cropland
16	38.770	96.300	cropland
17	37.390	98.360	cropland
18	48.580	98.140	cropland
19	37.200	115.840	barren

## 2. Data and Methodology

### 2.1. Data Set

A time series of 1-km NOAA 11 AVHRR data was acquired over 57 sites in the conterminous United States and parts of Canada for three growing seasons (April to October 1990–1992) by the U.S. Geological Survey [Hood, 1993]. It includes radiance measurements at the five AVHRR channels on the top of the atmosphere; three illumination/observation angles, namely, satellite viewing zenith angle (VZA), solar zenith angle (SZA), and relative azimuth angle (RAA); NDVI; and a pointer value that identifies the date and scene ID. The data were geometrically registered to map the pixels to correct ground locations. Radiometric calibration was also conducted which takes into account sensor degradation during the period 1990 to 1992 following the method of Teillet and Holben [1994].

The 57 sites were selected to represent various land cover types of homogeneity. Each 20 km  $\times$  20 km site is represented by 400 pixels. The 19 most uniform sites were selected for this study: seven for grassland, six for forest, five for cropland, and one for barren. Table 1 provides latitudes and longitudes of the upper left corners of the 19 sites and the corresponding surface characterization categories [Hood, 1993].

### 2.2. Cloud Screening

Since this study is concerned with clear-sky conditions only, overcast and cloud-contaminated pixels were screened out. Many algorithms have been proposed for detecting and classifying clouds using remotely sensed data [Coakley and Bretherton, 1982; Arking and Childs, 1985; Saunders, 1986; Gutman *et al.*, 1987; Saunders and Kriebel, 1988]. A four-step hybrid cloud-screening technique is used here that employs different algorithms to cope with different cloud conditions. The first step removes overcast pixels that do not meet one or more of the following criteria [Gutman *et al.*, 1987; Gutman, 1991]:

$$(R1 + R2)/2 < 35\% \quad (1)$$

$$R2/R1 > 1.3 \text{ (not for barren)} \quad (2)$$

$$T4 > 280 \quad (3)$$

where  $R1$  and  $R2$  denote the observed reflectance at channels 1 and 2 in percent, respectively, and  $T4$  the brightness temperature at channel 4 in degrees Kelvin. They are based on (1) cloud-free land surfaces are less reflective than clouds for both channels; (2) except for bare land, the clear-sky reflectance in channel 2 is significantly higher than that in channel 1 for most terrestrial surfaces; (3) clear scenes are generally warmer than clouds.

To identify partly cloudy pixels, a spatial coherence method is applied to those that were identified as being clear in the first step. This method was originally proposed by *Coakley and Bretherton* [1982] and has been widely used [e.g., *Gutman et al.*, 1987; *Saunders*, 1987]. The basis of this method is that the radiance of a cloud-contaminated scene is more variable than that of a clear scene. The validity of this method thus depends on surface uniformity. The fact that all the sites selected here are very homogeneous warrants the application of this method. To apply the spatial coherence method, background variabilities and standard deviations of  $R1$ ,  $R2$ , and  $T4$  were computed for the array of  $3 \times 3$  pixels surrounding each individual pixel. Background variability is defined as the minimum standard deviation in a given month. The thresholds of 1% and 1 K were selected for solar channels and thermal infrared channels, respectively. A pixel was considered to be contaminated by cloud, unless it satisfies all of the following criteria:

$$\delta R1 < \Delta R1 + 1.0\% \quad (4)$$

$$\delta R2 < \Delta R2 + 1.0\% \quad (5)$$

$$\delta T4 < \Delta T4 + 1.0 \text{ K} \quad (6)$$

where  $\delta$  and  $\Delta$  stand for standard deviation and background variability, respectively.

The third step makes additional use of  $T4$ . Considering that land surface temperature is subject to strong temporal and spatial variations, the criterion for channel 4 used in step 1 is quite crude. As a result, it may not effectively screen out cloud-contaminated pixels. On the other hand, however, it does not mislabel clear pixels as cloudy. For a given site, the criterion of  $T4$  is changed from 280 K to the sum of the mean  $T4$  and one standard deviation computed for those that were identified as being clear in steps 1 and 2 for the same site of  $20 \times 20$  pixels.

Finally, the image of cloud-free pixels produced with the above procedures was further subject to visual inspection to discard some apparently misidentified pixels. This was done with the aid of analyzing a time series of NDVI, in view of the fact that NDVI does not change dramatically with time and that the presence of cloud tends to reduce the value of NDVI. Thus if a NDVI is obviously too low with reference to the time series of NDVI, the observation was removed. This step generally eliminated low thin clouds and fog. Unlike previous steps, this step is not automatic (no objective rule applied), as it relied partially on one's experience of image analysis. It is, however, not responsible for the removal of the majority of cloudy pixels.

While the percentage of clear pixels that survive from the tests varies with time and site, it was generally less than 30%. This number may be lower than the actual frequency of

clear-sky occurrence, resulting from imposing the conservative criteria. After cloud screening, the reflectances of all clear pixels over a test site were averaged and the mean values over the same sites were employed in the BRDF study. Inasmuch as the sites were homogeneous, the BRDF that is derived from the averaged reflectances should be applicable to the individual AVHRR pixels.

### 2.3. Methodology

For an empirical study of BRD it would be ideal to have the same target viewed from different directions at the same time. Unfortunately, the AVHRRs cross-track scanning allows one observation at a time from a single direction. One must therefore resort to the observations obtained over different regions of the same surface condition. The dependency of BRD on SZA can be investigated by making use of a time series of data during a period over which surface does not change significantly but SZA does. Differences in location and time result in a variety of satellite-Sun-target geometry. So long as surface conditions are the same or similar enough, the measurements made for different time and locations can be considered together for BRD analysis.

Typical AVHRR viewing and illumination characteristics were illustrated by *Holben and Fraser* [1984]. Satellite VZA varies in proportion to scan angle, ranging from  $0^\circ$  at nadir to  $\pm 69^\circ$  for extreme off-nadir viewing. SZA which changes with time and location decreases by up to  $20^\circ$  when a site is viewed from backward to forward directions over a certain period, as shown in Figure 1a. The points with the same symbol in Figure 1 represent clear-sky observations obtained over a period during which the change of reflectance due to the temporal variation of surface condition is expected to be small compared to the change due to the effect of BRD. Such a period is typically set to 1 month, but it is somewhat longer in the middle of summer (June and July) and shorter in early spring and late fall. NDVI serves to determine the duration of the period during which NDVI is relatively constant and the number of the AVHRR measurements is sufficient to ensure that the composite includes a wide range of viewing angles. The cases shown in Figure 1 represent a whole growing season. For brevity a cluster of points with the same symbol are regarded as being from a "pseudo" scan line, i.e., the same target observed at different angles under the same atmospheric conditions.

It follows from Figure 1a that the solar and satellite viewing zenith angles are not completely independent, which is unfavorable for the BRD study. The dependence is due to the AVHRR observation patterns, i.e., the backscattering observations of negative VZAs were collected at high SZAs, while the forward scattering measurements of positive VZAs were made for low SZAs. Fortunately, the range of the variation in SZA in a pseudo scan line is not very large. Figure 1b illustrates the variations of RAA with VZA. It appears that RAA does not depend on VZA but on SZA. Moreover, the measurements were made close to the principal plane (within  $40^\circ$ ) for a growing season. Therefore the dependence of reflectance on RAA is not investigated in this study.

## 3. Effects of Different Factors on Bidirectional Reflectance Distributions (BRD)

### 3.1. Surface Type

Figure 2 shows the variation in cloud-free visible and near-infrared reflectances with VZA over four land cover

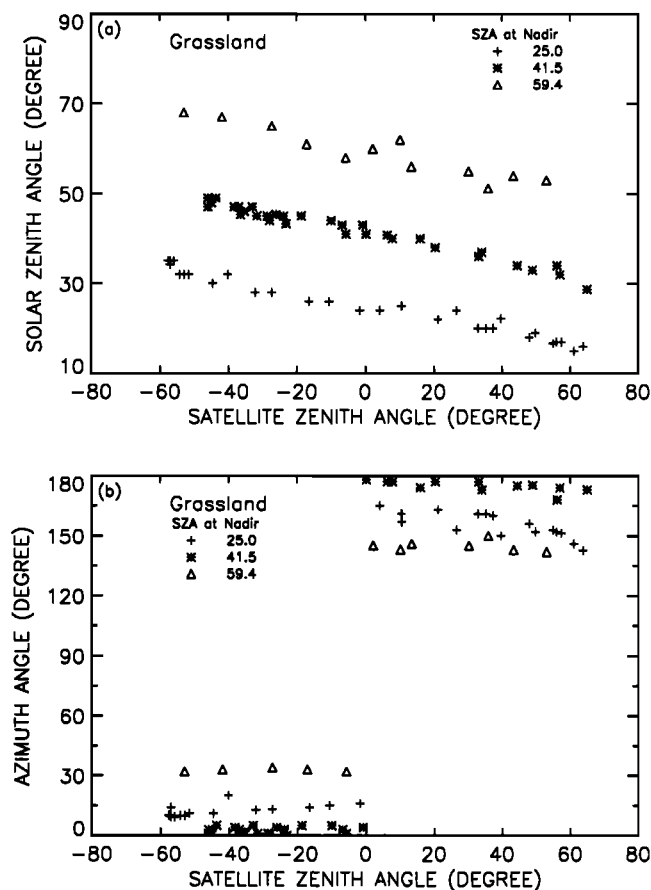


**Figure 1.** The variations of (a) solar zenith angle and (b) the relative azimuth angle with satellite zenith angle at a grassland site. Negative and positive satellite zenith angles correspond to backward and forward scattering, respectively. Solar zenith angles (SZA) for nadir measurements are given in the plots. A cluster of points falling along a line were treated as if they were from a single scan line, though they actually span some time.

types. Also shown in Figure 2 are the standard deviations of the site mean reflectances. They are generally less than 2 to 3%, much lower than the mean reflectances, indicating the homogeneity of the selected sites. SZA and NDVI given in Figure 2 correspond to the nadir values. The reflectances of the four land types differ in several respects. First, the magnitudes of reflectance in both channels and their differences are very different among the four land cover types. Second, the angular variation of reflectance with VZA depends on surface type, although strong backscattering is manifest in all four cases. Backscattering peaks at VZA close to SZA (hot spot). For barren and grassland, reflectance decreases in the direction away from hot spot with minima occurring at the extreme forward scattering angles. The surface BRD for bare soil measured by *Kimes et al.* [1984] and *Kimes and Sellers* [1985] also exhibits similar features. This phenomenon is due to the relatively opaque soil vertical structures that cause dark shadows [*Kimes*, 1983]. The hot spot effect for cropland and forest is due to the fact that shadows cast by the canopies is minimum in the solar direction. Therefore as VZA approaches the sun direction, the size of shadows become progressively smaller

[*Hapke*, 1981; *D'Iorio et al.*, 1991]. The phenomenon was also observed by *Kimes et al.* [1986] on the ground for a stand of scrub pine. The effect of hot spot weakens rapidly as the azimuth plane moves away from the principal plane [*Kimes et al.*, 1986; *Li and Strahler*, 1986; *Jupp and Strahler*, 1991]. As the AVHRR data used in this study are not obtained exactly in the principal plane (Figure 1b), the observed hot spot effect is not the strongest. The BRD effects for barren and grassland are significantly stronger than for cropland and forest. The angular dependence of reflectance for grassland (Figure 2b) bears a strong resemblance to that for barren (Figure 2a). This is mainly because the grassland shown in Figure 2b contains sparse grass with small NDVI (0.13); that is, a significant area of soil may not be covered by vegetation. Thus the scattering properties of the background soil increase in importance.

### 3.2. Normalized Difference Vegetation Index (NDVI)

Figure 3 shows the angular variations of visible and near-infrared reflectance over grassland obtained at the same SZA but with different NDVIs. The curves are polynomials fitted to the data, with  $S_d$  denoting the standard deviation of the fitting to the reflectance measurements (generally below 1%). The magnitudes of reflectance in both channels are sensitive to NDVI for small SZA, whereas channel 1 reflectance is much less sensitive to NDVI when SZA is large. This is because the TOA reflectance of channel 1 is modified considerably by Rayleigh scattering. As the SZA increases, contribution of the Rayleigh scattering to the TOA reflectance becomes more dominant and thus the surface contribution is obscured. At small SZAs, large discrepancies exist in the reflectances of both channels due to the natural variability of the surface morphological and reflectance properties. The effect of NDVI on BRD is also evident. For NDVI = 0.13, the reflectances at both channels have strong peaks around the hot spot regions and then diminish monotonically. For large NDVI the curves become relatively flat and the hot spots are weak. Yet, the hot spot takes place at a VZA larger than SZA as NDVI increases. For large NDVI the hot spot is determined not only by SZA but also by the orientation of the majority of leaves [*Gao*, 1993]. The angular variation pattern of BRD for NDVI = 0.53 is very different from that for NDVI = 0.13.

The results for cropland are shown in Figure 4. In contrast to grassland the hot spot for near-infrared channel strengthens as NDVI increases. Recent modeling studies showed that the hot spot effect increases with increasing leaf dimension [*Jupp and Strahler*, 1991] and the distances between leaves [*Ross and Marshak*, 1988] or with decreasing leaf transmittance [*Li and Strahler*, 1986]. Presumably, the increase of NDVI for cropland is mainly associated with enlarging the size of leaves, whereas the increase of NDVI for grassland may be primarily due to narrowing the distances between leaves and diminishing the background effects. In this case, the response trend of the hot spot effect to change in NDVI over grassland would be opposite to that over cropland. The discrepancies in BRD between grassland and cropland also arise from the differences in their physical and optical properties. For example, the near-IR reflectance of a grass leaf is lower than its transmittance [*Blad*, 1988], while the reflectance of a crop leaf is generally higher than its transmittance [*Ross and Marshak*, 1988]. Therefore for a moderate NDVI the reflectance over grassland is influenced

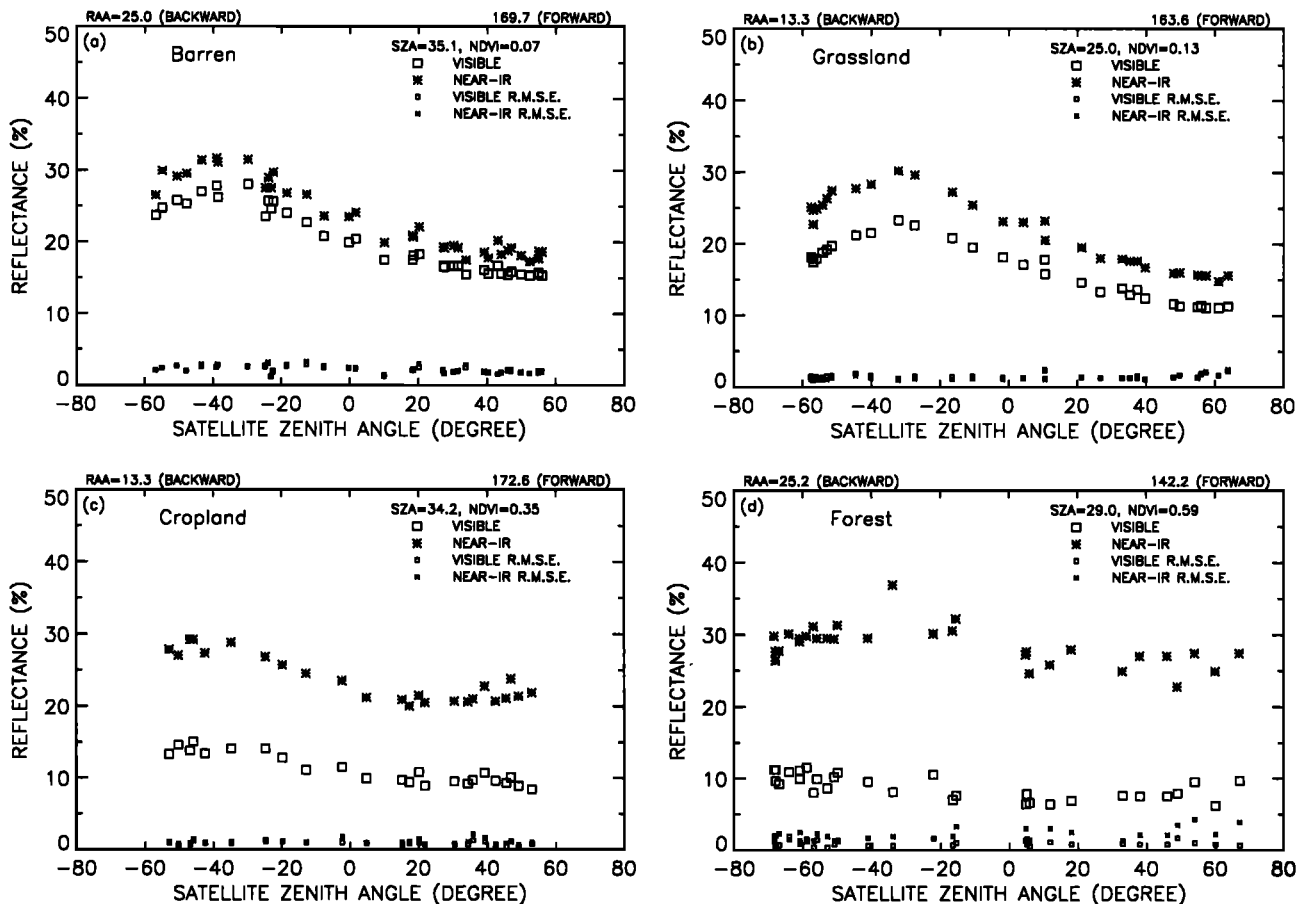


**Figure 2.** Site-mean reflectances for advanced very high resolution radiometer (AVHRR) visible and near-IR channels versus satellite zenith angle over (a) barren, (b) grassland, (c) cropland, and (d) forest. The points near  $X$  axes are the standard deviations of the individual reflectances measured over a site.

more by the area of the underlying soil exposed to the satellite sensor, whereas the reflectance over a cropland is determined more by the leaves. For a complete coverage of canopy with large NDVI, the large reflectances of crop leaves result in asymmetric BRDs; that is, the reflectance is larger in the backscattering directions. Over a grassland of large NDVI the high transmittance of grass leaves leads to more symmetric BRDs because of increasing diffuse illumination. This suggests that NDVI cannot account for the difference in the characteristics of BRD among different land cover types. Thus different BRDFs need to be developed over individual land cover types.

Figure 5 shows the results for forests. Note that the change of NDVI over forest is caused mainly by the variation of the reflectance in channel 2, since the reflectance in channel 1 is quite stable. The angular variation of channel 2 reflectance is stronger than channel 1. In general, the BRD for forest behaves more like cropland, but the hot spot effects for forest are not so strong as for cropland.

### 3.3. Solar Zenith Angle (SZA)

BRD is known to be dependent on SZA. Figure 6 demonstrates the effect of SZA on BRD for (a) barren, (b) grassland, (c) cropland, and (d) forest. The variations of both visible and near-IR reflectances are presented for all land cover types except for barren whose reflectances in the two channels are very similar in trend and magnitude. It follows

from Figure 6a that the hot spot is much more marked over barren than over vegetated lands. The shift of hot spot follows closely the Sun position. According to *Cierniewski and Courault* [1993] the BRD of a soil surface is strongly influenced by the physical structure of soil material, the size, and orientation of elementary facets. These tiny facets create microscale irregularities on the soil surface and cause shadowing of solar illumination in all directions but around toward the Sun. Since the AVHRR viewing geometry is not always in the principal plane (Figure 1b), the VZAs of the backscattering peaks are not exactly coincident with SZAs.

The responses of the BRDs for three vegetated lands to SZA are qualitatively similar but differ considerably from that for barren. It appears that the dependencies of the reflectance in both channels 1 and 2 on VZA intensify with increasing SZA. It is interesting to note that reflectance appears to be independent of SZA when the vegetated targets are observed in a forward direction with a VZA around  $20^\circ$ . Comparison of Figure 6 to Figures 3–5 suggests that SZA has a smaller effect on BRD than NDVI.

## 4. Development of BRD Functions (BRDF)

The above analyses of the observed BRDs suggest that a BRDF for AVHRR data should be a land-cover-dependent function of viewing geometry, SZA, and NDVI. By surveying and testing various formulas proposed for the BRDF, we

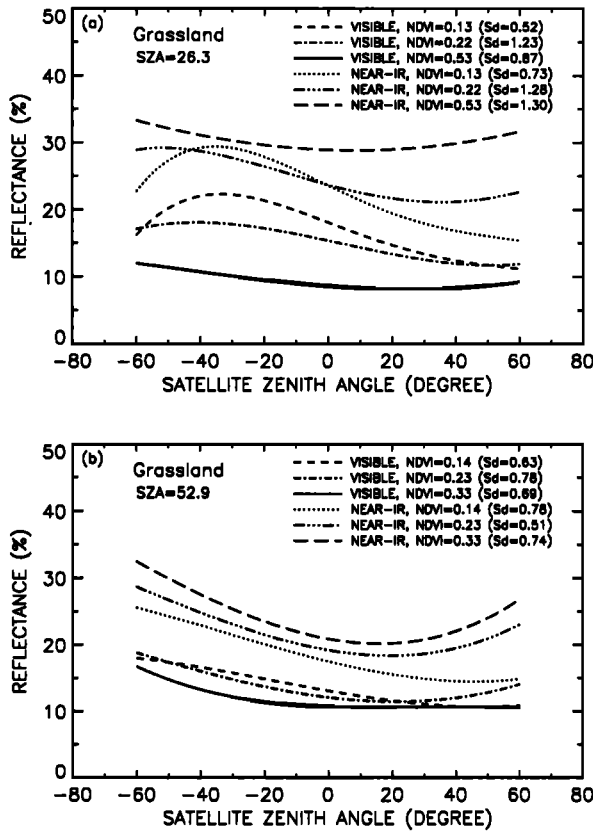


**Figure 3.** The dependencies of top-of-atmosphere (TOA) visible and near-IR reflectances on satellite zenith angle for different normalized difference vegetation index (NDVI) over grassland at (a) SZA = 26.3 and (b) SZA = 52.9. The curves are the polynomial fittings to scatter data, with the standard difference between observed and fitted reflectances given by Sd.

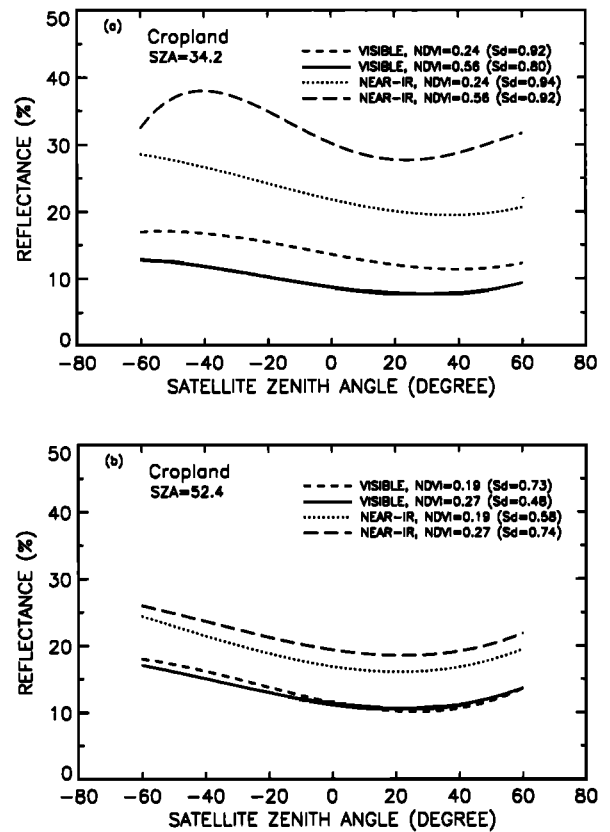


**Figure 4.** Same as Figure 3 but over cropland at (a) SZA = 34.2 and (b) SZA = 52.4.

decided to develop a set of BRDFs based on the physically based model of *Roujean et al.* [1992a] because it had some unique features suitable for addressing our problem. First, the model is derived from geometric consideration of the scattering process in a canopy. As a result, it is expected to have a plausible dependency on, among others, relative azimuth angle. This is particularly important for this study, since the AVHRR data under study do not contain enough range of RAA to determine empirically such a dependency. Second, the model contains approximately the same number of parameters as were identified in the above analyses, namely, three geometric parameters and one physiological canopy parameter. The physiological parameter used in their model is the leaf area index (LAI) instead of NDVI; however, these two parameters are correlated [*Spanner et al.*, 1990]. Third, their model is designed to be applicable to heterogeneous surfaces. Again this is important, as our goal is to develop the BRDFs for different land cover types.

A concern on validity may arise from the fact that the model of *Roujean et al.* [1992a] was for surface BRDF, whereas the BRDF to be developed here is at the TOA. Some studies [*Kimes and Sellar*, 1985; *Roujean et al.*, 1992b] have shown that the anisotropic properties of the surface dominate over the impact of the atmospheric anisotropy. The bidirectional dependencies of AVHRR are due essen-

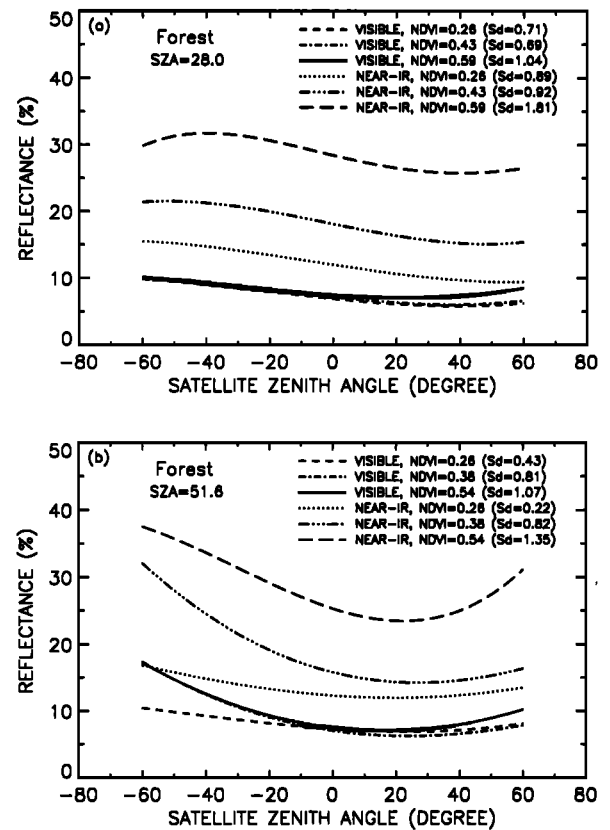


**Figure 5.** Same as Figure 3 but over forest at (a) SZA = 28.0 and (b) SZA = 51.6.

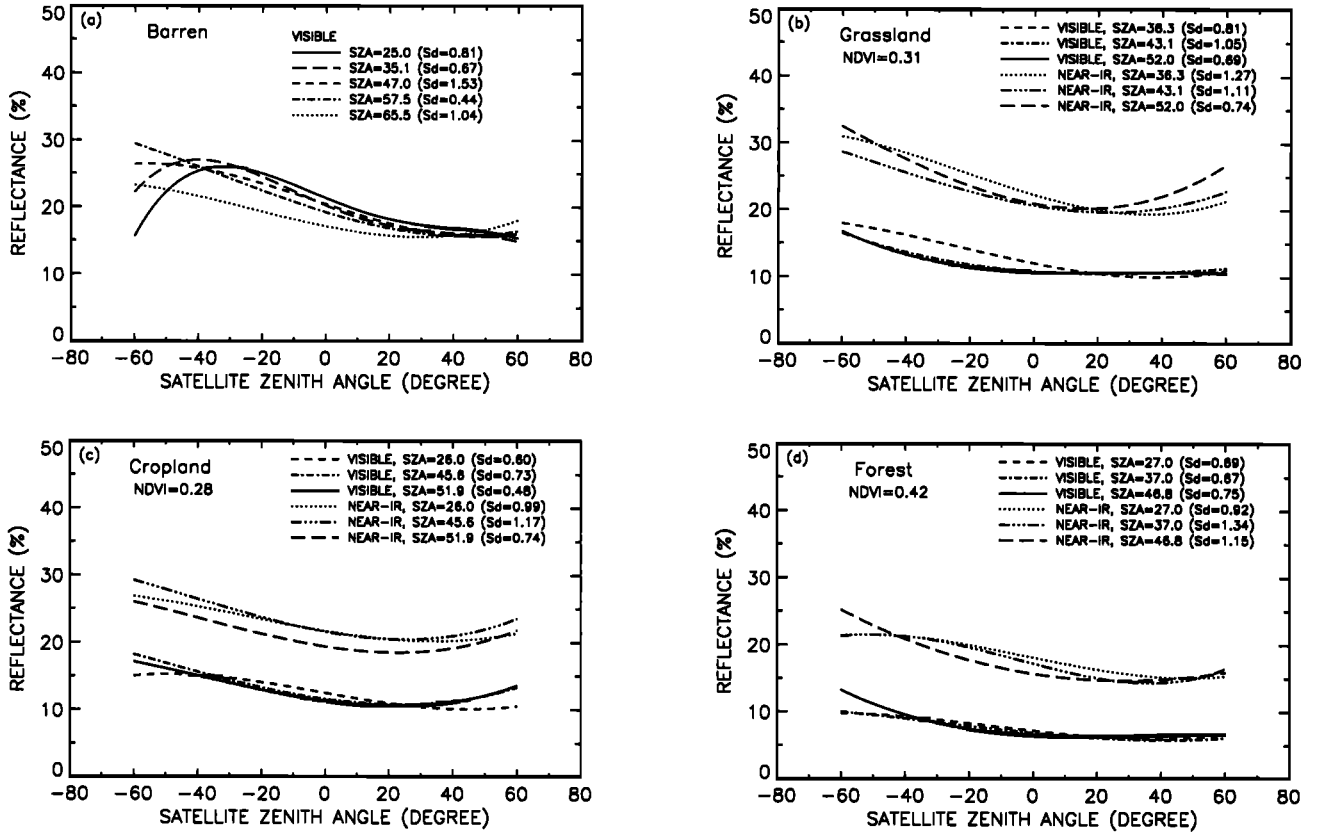


**Figure 6.** The dependencies of TOA visible and near-IR reflectances on satellite zenith angle at different SZAs of the same NDVI over (a) barren, (b) grassland, (c) cropland, and (d) forest. For barren land, only visible reflectances are presented.

tially to surface effects. This appears to be supported by the qualitative resemblance between the BRDs presented in this paper and those derived from the surface measurements over a bare soil by *Kimes and Seller* [1985], over grasslands by *Kimes et al.* [1984] and *Deering and Middleton* [1990], and over a forest by *Kimes et al.* [1986]. However, the above argument may not hold for other satellite data with lower spatial resolutions. In fact, an opposite conclusion that the TOA BRD is mainly controlled by the atmospheric anisotropy was reached from the studies using the Earth's radiation budget satellite data with the resolution of tens of kilometres [*Pinker and Stowe*, 1990; *Li and Garand*, 1994]. Apart from satellite resolution the relative importance of the surface and the atmosphere in effecting TOA BRD depends on climate regime. It is expected that atmospheric effects on TOA BRD are larger for a humid and hazy atmosphere than for a dry and clean one. In any case, the validity of a BRDF rests on whether it fits well the AVHRR observations. The fitted coefficients may depend somewhat on climate.

The model of *Roujean et al.* [1992a] is expressed as

$$R_i(\theta_s, \theta_v, \phi) = K_0 + K_1 f_1(\theta_s, \theta_v, \phi) + K_2 f_2(\theta_s, \theta_v, \phi) \quad (7)$$

where

$$f_1(\theta_s, \theta_v, \phi) = \frac{1}{2\pi} [(\pi - \phi) \cos \phi + \sin \phi] \text{tg} \theta_s \text{tg} \theta_v$$

$$- \frac{1}{\pi} (\text{tg} \theta_s + \text{tg} \theta_v + \sqrt{\text{tg}^2 \theta_s + \text{tg}^2 \theta_v - 2 \text{tg} \theta_s \text{tg} \theta_v \cos \phi}) \quad (8)$$

$$f_2(\theta_s, \theta_v, \phi) = \frac{4}{3\pi(\cos \theta_s + \cos \theta_v)} \cdot \left[ \left( \frac{\pi}{2} - \xi \right) \cos \xi + \sin \xi \right] - \frac{1}{3} \quad (9)$$

$$\cos \xi = \cos \theta_s \cos \theta_v + \sin \theta_s \sin \theta_v \cos \phi \quad (10)$$

where  $R_i$  denotes the reflectance in channel 1 ( $i = 1$ ) and channel 2 ( $i = 2$ );  $\theta_s$  and  $\theta_v$  are the Sun and satellite viewing zenith angles (from  $0^\circ$  to  $90^\circ$ ), respectively;  $\phi$  is the relative azimuth angle between solar and sensor directions, ranging from  $0^\circ$  for backward scattering to  $180^\circ$  for forward scattering;  $f_1$  gives the bidirectional dependency due to diffuse reflection from opaque reflectors on the ground and to the shadowing effects of the leaves;  $f_2$  accounts for the contribution to BRD of the volume scattering by a collection of randomly dispersed facets of canopies and bare soils. Note that  $\theta_s$  and  $\theta_v$  are reciprocal in  $f_1$  and  $f_2$  and thus in  $R_i$  as well; that is, their values remain the same by exchanging the values of  $\theta_s$  and  $\theta_v$ .  $K_0$  represents the bidirectional reflectance for  $\theta_s = \theta_v = 0$ .  $K_1$  and  $K_2$  measure the contributions of  $f_1$  and  $f_2$ . In the model of *Roujean et al.* [1992a],  $K_0$ ,  $K_1$ , and  $K_2$  were given as functions of parameters pertaining to

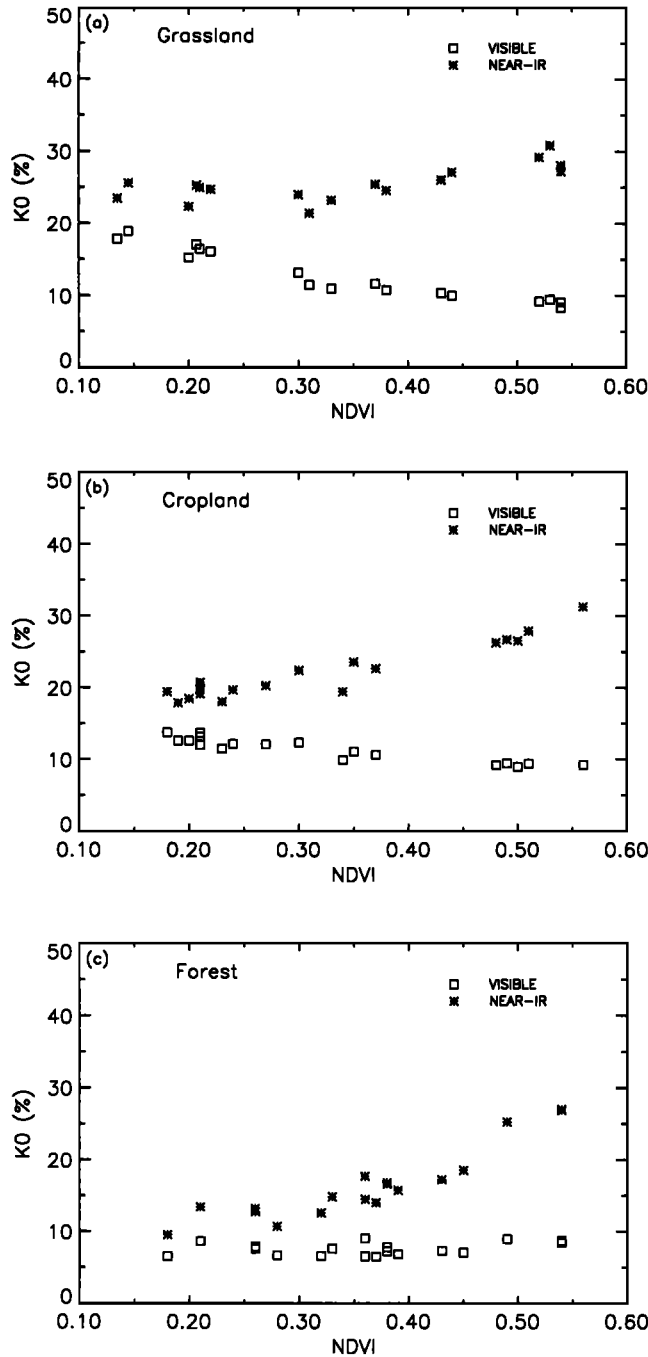


**Figure 7.** Variations of the coefficient  $K_0$  in a bidirectional reflectance distribution function (BRDF) with NDVI for (a) grassland, (b) cropland, and (c) forest.

the physical structure and optical properties of a reflecting media as well as LAI. To the first approximation we can assume that the physical structure and optical properties are land cover type-specific. As a result,  $K_0$ ,  $K_1$ , and  $K_2$  are modified solely by LAI which can be related to NDVI for a given type of land cover [Sellers, 1985].

The coefficients  $K_i$  were thus determined empirically as functions of NDVI for each land cover type. To do so, (7)–(10) were first applied to the AVHRR data. The values of  $K_0$ ,  $K_1$ , and  $K_2$  were computed by minimizing the differences between the observed and the modeled reflectances using an optimization algorithm. The relationships between

these coefficients and NDVI were investigated for each land cover type. In line with the above analysis the coefficients are found to depend strongly on NDVI for vegetated land. Figure 7 shows, for example, the dependency of  $K_0$  on NDVI. Note that  $K_0$  for channel 2 is more sensitive to NDVI than for channel 1 over cropland and forest, while  $K_0$  is sensitive to NDVI for both channels over grassland. The analytical functions of the coefficients versus NDVI were determined by a curve-fitting software. Table 2 delineates the functions of  $a_{1i} = K_1/K_0$  and  $a_{2i} = K_2/K_0$  where  $i = 1, 2$  representing AVHRR channels 1 and 2, respectively;  $a_{1i}$  and  $a_{2i}$  correspond to the coefficients of an anisotropic factor ( $\Omega$ ) obtained by normalizing equation (7) to the nadir ( $\theta_v = 0$ ) for the overhead Sun ( $\theta_s = 0$ ),

$$\Omega_i(\theta_s, \theta_v, \phi) = \frac{R_i(\theta_s, \theta_v, \phi)}{R_i(0, 0, \phi)} = 1 + a_{1i}f_1(\theta_s, \theta_v, \phi) + a_{2i}f_2(\theta_s, \theta_v, \phi) \quad (11)$$

noting  $R_i(0, 0, \phi) = K_0$ ;  $a_{11}$  and  $a_{12}$  are set to zero for cropland and forest, as the least squares fits lead to negative values of small magnitudes due to the noise and small volume of the data set. This is consistent with Roujean et al. [1992a] who obtained very small  $K_1$  for the same two types of surfaces by fitting their model to the surface bidirectional reflectance measurements made by Kimes [1983] and Kimes et al. [1986]. As an overall measure of the statistical significance of the fitting, root-mean-square (RMS) differences between observed and modeled reflectances are presented in Figure 8. The RMS differences are generally less than 2%, typically around 1%. Weak dependencies of the differences on NDVI suggest that the functions successfully account for the effects of NDVI.

To further demonstrate the potential of using a set of simple functions for BRDF, Figures 9–12 compare observed and modeled visible and near-infrared reflectances for the four surface types of interest. The modeled values were obtained from the BRDF model given by (11) and Table 2, and  $K_0$ . A constant  $K_0$  indicated in the plot was used for each panel of Figures 9–12. In theory,  $K_0$  should be independent of SZA as well as viewing angles for the same target

**Table 2.** Coefficients of BRDFs Developed for AVHRR Measurements at Channels 1 and 2 Over Land Surfaces Under Clear Conditions

Surface Type	Channel 1	
	$a_{11}$	$a_{21}$
Barren	0.210	1.629
Cropland	0.0	$3.622\text{NDVI}^{0.539}$
Forest	0.0	$3.347\text{NDVI}^{0.153}$
Grassland	$1.335e^{-11.39\text{NDVI}}$	$-0.493 + 14.94\text{NDVI} - 18.32\text{NDVI}^2$
Surface Type	Channel 2	
	$a_{12}$	$a_{22}$
Barren	0.212	1.512
Cropland	0.0	$1.620\text{NDVI}^{0.109}$
Forest	0.0	$1.830\text{NDVI}^{-0.105}$
Grassland	$7.745e^{-22.80\text{NDVI}}$	$-0.250 + 13.88\text{NDVI} - 20.43\text{NDVI}^2$

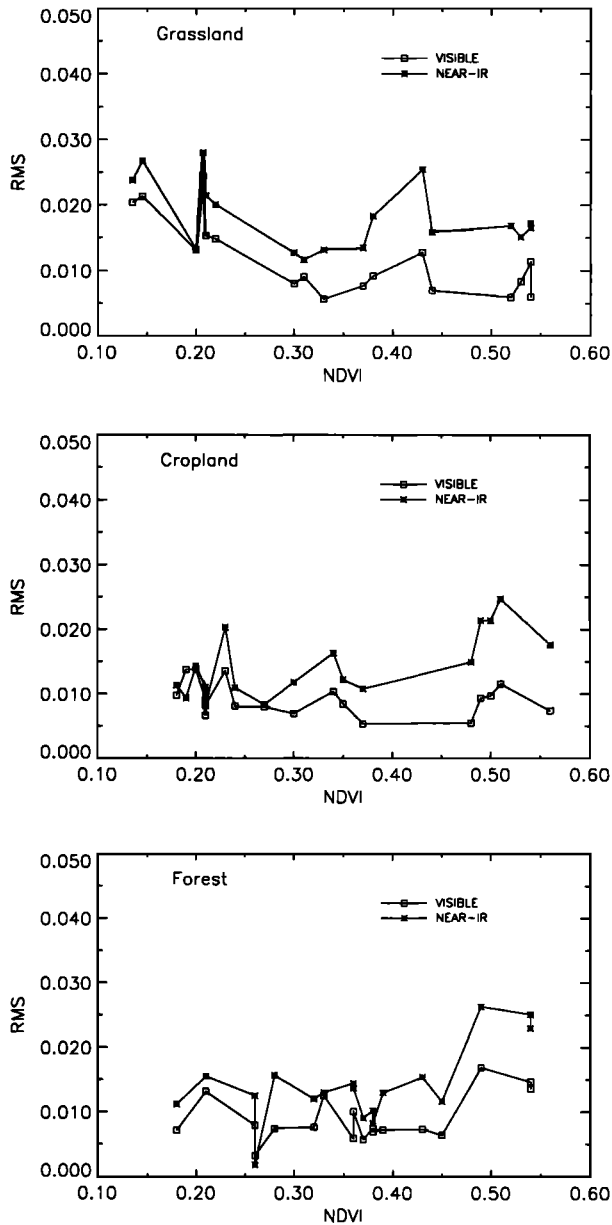


**Figure 8.** Root-mean-square (RMS) differences between observed and modeled reflectances in the visible and near-infrared channels of AVHRR, as functions of NDVI.

of the same condition. The barren land shown in Figure 9 is a fixed site with little seasonal changes and thus the values of  $K_0$  determined at different SZAs are very close. For vegetated land,  $K_0$  depends on NDVI, the AVHRR channel, and land cover type, as shown in Figure 7. For the same type of vegetated land with similar NDVI, the values of  $K_0$  are found to be similar. The values of SZA and NDVI used to produce the modeled reflectances in Figures 9–12 correspond to individual measurements; they may differ somewhat from those appearing in the plots for the nadir measurements. Since the BRDF for barren land is a function of three angles, the comparisons shown in Figure 9 are for various SZAs ranging from 25.0° to 65.5°. For vegetated land surfaces, such comparisons are selected that have significant differences in SZA and NDVI.

In general, the modeled results agree rather well with the observations. The BRDF appears to be able to model the evolution of a BRD in response to changing SZA and NDVI. One may regard the difference between the maximum and the minimum reflectances as the signal of the bidirectional effect. The corrections made by these BRDFs are thus significant in that the noise represented by the discrepancies between modeled and observed reflectances is much smaller than the signal. The good agreements suggest that a single BRDF is sufficient to correct for the bidirectional dependencies on SZA and NDVI for a given land cover type. It is not surprising to find some disagreements, as the basic functions given by (8) and (9) were derived on the basis of a simple physical model for some idealized canopy conditions. Large disagreements generally occur around the hot spot regions for small SZAs. When SZA is small, the contribution of the lower canopy to the TOA BRD increases due to more illumination being available. The model of *Roujean et al.* [1992a] does not, however, account for the contribution of the lower canopy which produces different BRD from the upper canopy. As for barren, the failure to allow the macroscale irregularities of a soil surface in the model of *Roujean et al.* [1992a] might explain the poor agreement near the hot spot region at small SZAs.

## 5. Application of BRDF in Land Monitoring

As stated in the introduction, AVHRR data can be used to monitor the temporal variation of land targets after the bidirectional dependencies have been removed. When a BRDF is available, there are two means of eliminating the bidirectional effects. One is to normalize the measurements made at a variety of angles to a common Sun-target-satellite geometry. Such a geometry is often selected to be the viewing angle of 0° (nadir) at the SZA of 45° [e.g., *Gutman*, 1994]. Based on the BRDF of (11), one can infer the reflectance at any Sun-target-satellite geometry,  $R_i(\Theta_s, \Theta_v, \Phi)$ , from an observed reflectance  $R_i(\theta_s, \theta_v, \phi)$  by

$$R_i(\Theta_s, \Theta_v, \Phi) = \frac{\Omega_i(\Theta_s, \Theta_v, \Phi)}{\Omega_i(\theta_s, \theta_v, \phi)} R_i(\theta_s, \theta_v, \phi) \quad (12)$$

The inferred reflectances for common Sun-target-satellite geometry are particularly useful for detecting the temporal evolution of surfaces, since the dependencies on both the viewing geometry and the SZA are removed. Hence the changes in normalized reflectance are due primarily to the variations of surface properties, if the atmosphere does not vary considerably.

Another approach is to derive an albedo defined over the complete viewing domain of the upward hemisphere from a reflectance measurement by

$$A_i(\theta_s) = \frac{R_i(\theta_s, \theta_v, \phi)}{\Omega_i(\theta_s, \theta_v, \phi)} \int_0^{2\pi} \int_0^{\pi/2} \cdot \Omega_i(\theta_s, \Theta_v, \Phi) \cos \Theta_v \sin \Theta_v d\Theta_v d\Phi \quad (13)$$

where  $\theta_s$  is the actual SZA of the measurement. The integration of (13) can be easily carried out numerically. While albedo is less useful than the normalized reflectance for monitoring the changes of surface conditions due to its dependency on SZA, it is an important geophysical param-

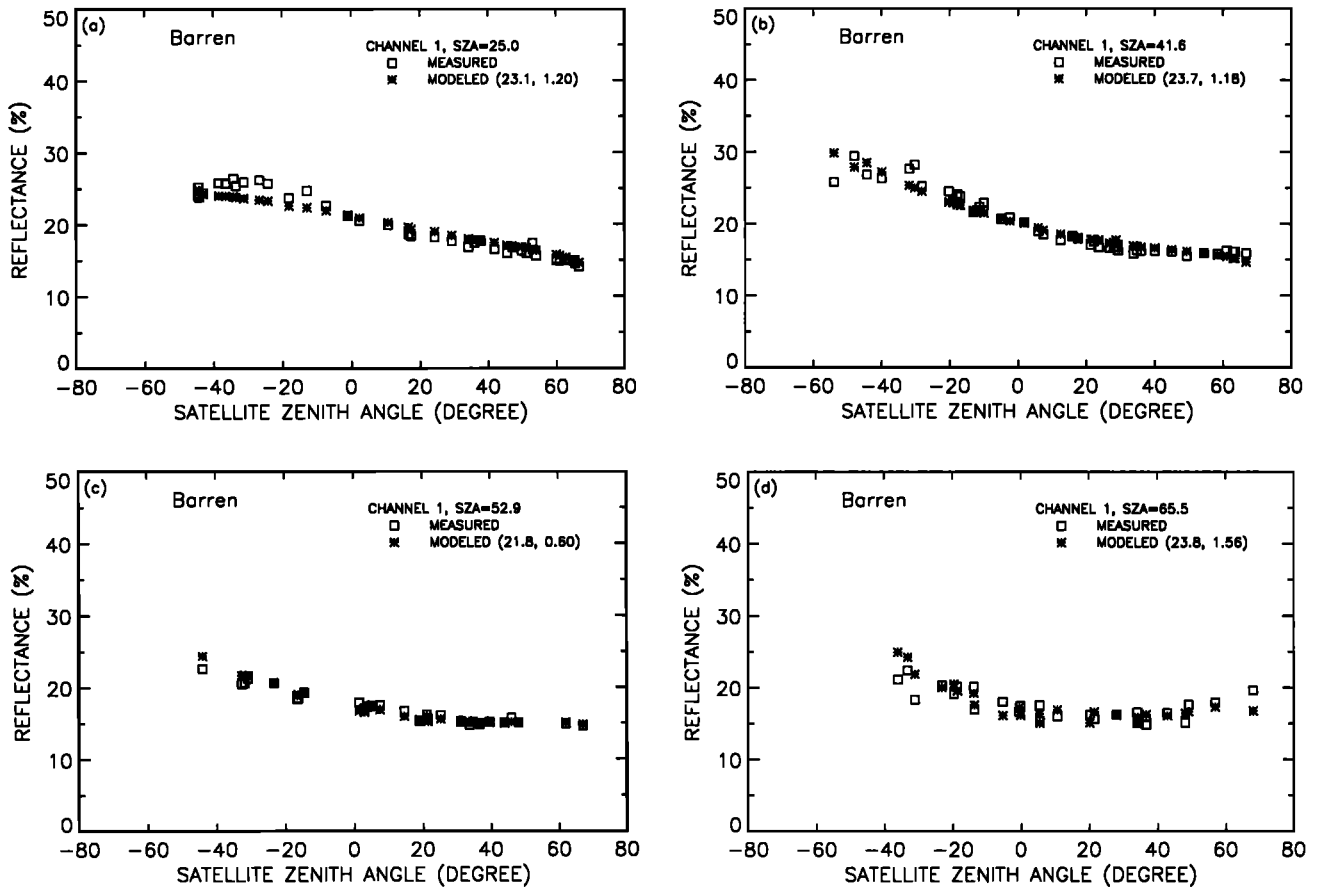


**Figure 9.** Comparisons of the observed and modeled visible reflectance over barren at different SZAs. The first number in parentheses appearing beside “MODELED” is the  $K_0$  used in modeling and the second is the standard difference between observed and modeled reflectance.

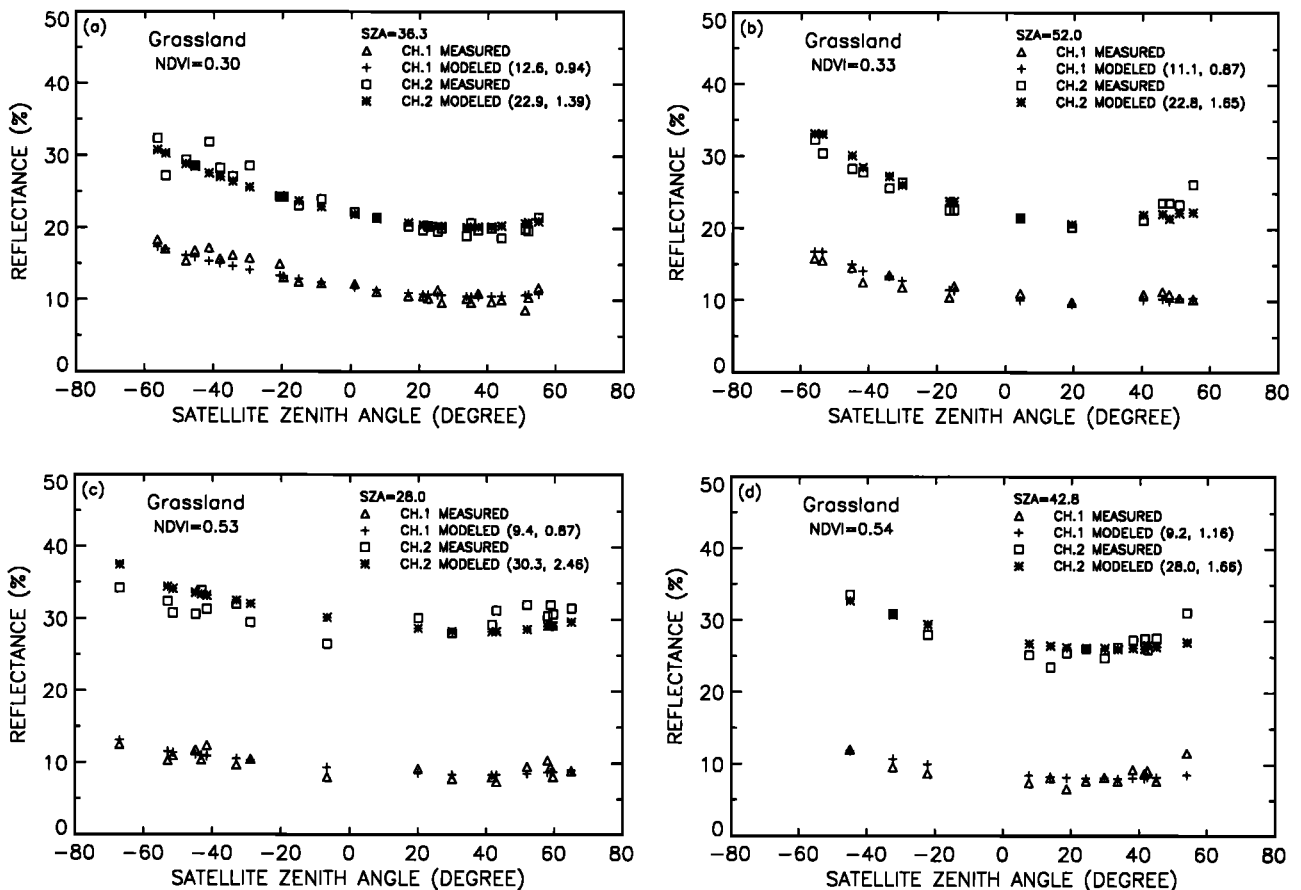


**Figure 10.** Same as Figure 9 but over grassland for different NDVIs and SZAs.

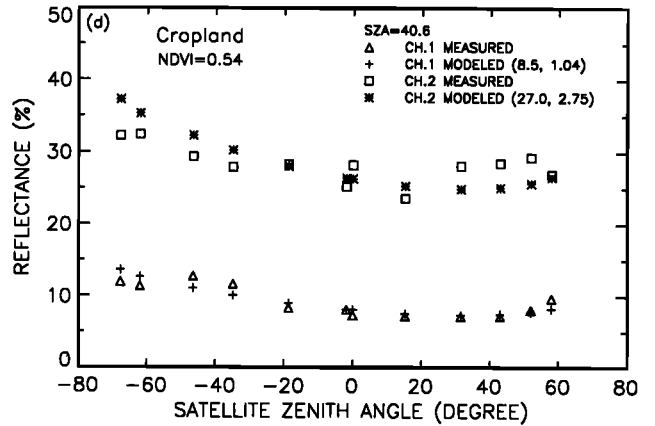
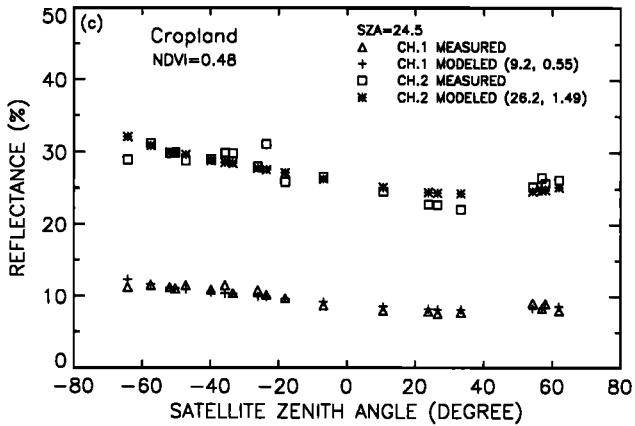
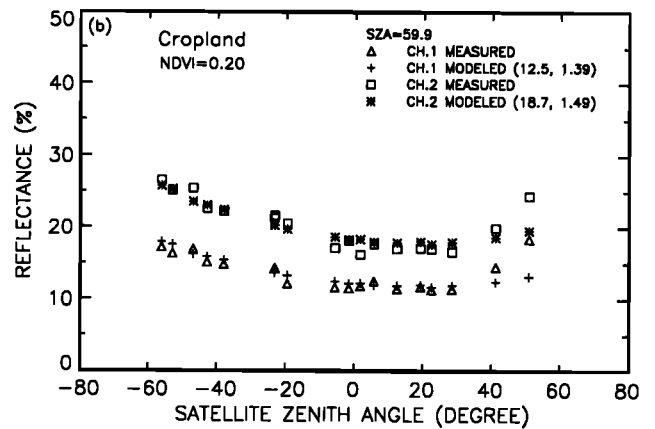
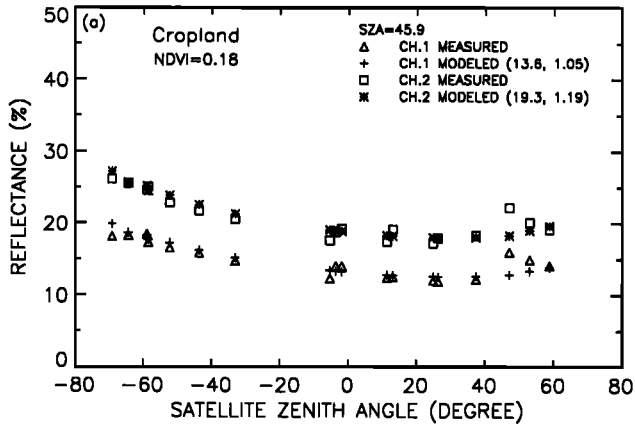


Figure 11. Same as Figure 10 but over cropland.

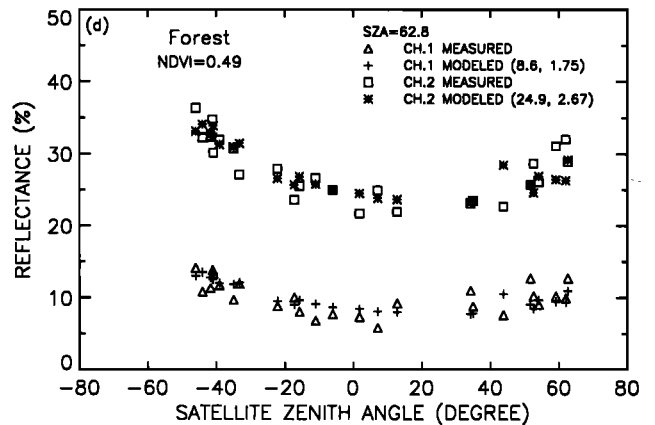
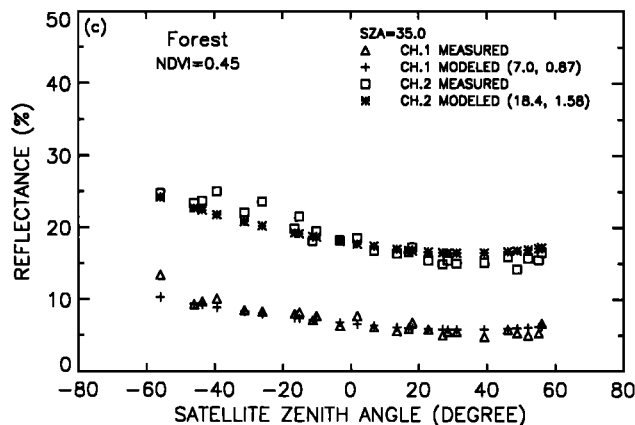
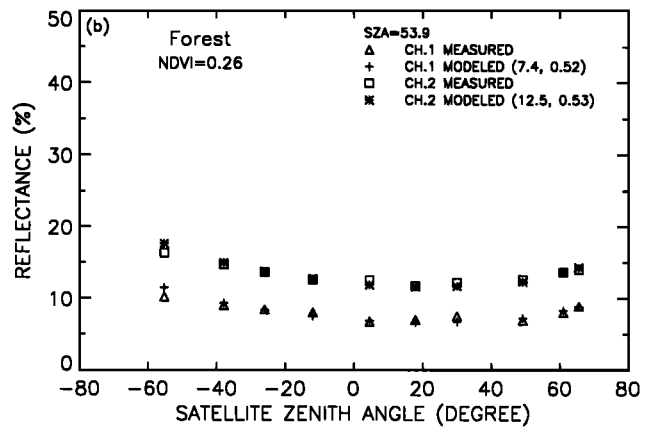
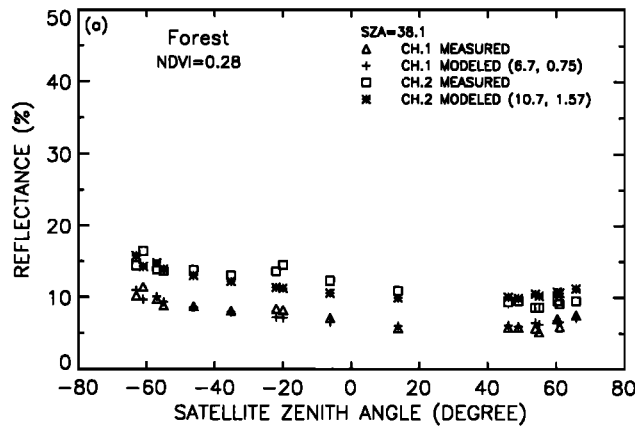
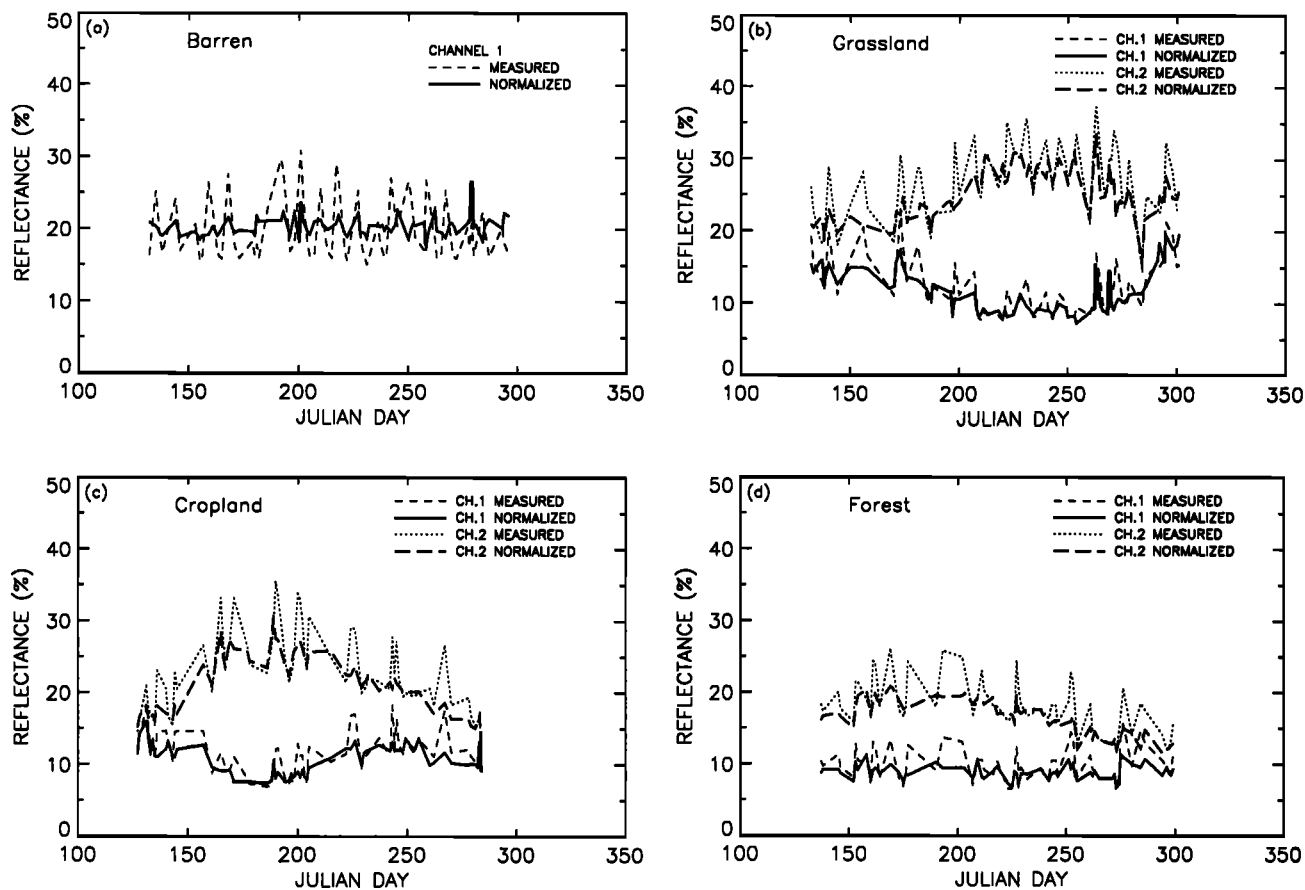


Figure 12. Same as Figure 10 but over forest.



**Figure 13.** Seasonal variations of the original AVHRR reflectance and normalized reflectance at nadir viewing angle for  $SZA = 45^\circ$  Sun over (a) barren, (b) grassland, (c) cropland, and (d) forest.

eter modulating the energy budget of the Earth-atmosphere system. TOA visible albedo is also needed for retrieving many surface parameters such as the photosynthetically active radiation absorbed by plant canopies [Li and Moreau, 1995].

As an example, Figure 13 compares the seasonal variations of the original AVHRR reflectances measured over four land cover types with the reflectances normalized to  $SZA = 45^\circ$  according to the BRDFs developed. The cloud-free time series data for the 1991 growing season were used. It is seen that the original reflectances exhibit strong temporal variations of long and short timescales. The long-term variations are mainly associated with the seasonal changes of canopy greenness for vegetated land, indicated by the difference between channels 1 and 2. In contrast to vegetated land, barren has no apparent seasonal regime. There are strong short-term oscillations of quasi-period in original reflectances for all land cover types. The quasi-period is very close to the 9-day period of AVHRR viewing geometry [Gutman, 1989]. It is thus concluded that the oscillations arise from the bidirectional dependencies of AVHRR data. The oscillations are significantly suppressed in normalized reflectance following the correction for BRDF effects. The remaining small fluctuations could be due to errors in BRDF and  $K_0$ , variations in atmospheric conditions (water vapor, aerosols), and residual cloud effects. It is likely that changes in atmospheric conditions may result in large fluctuations in the normalized reflectance over the regions with different

climate regimes. In addition, the remaining fluctuations tend to strengthen with greenness, suggesting that the effects of greenness on BRDF have not been totally accounted for by the use of NDVI.

## 6. Summary

An AVHRR data set of 3 years over 19 land target sites (20 km for each site) in the conterminous United States and parts of Canada was used to examine the bidirectional reflectance distributions (BRDs) for visible and near-infrared measurements from AVHRR. Uniform sites of barren, grassland, forest, and cropland were selected. Since the study is restricted to clear skies, cloud-screening techniques were applied to eliminate overcast and cloud-contaminated pixels. Observed top-of-atmosphere (TOA) reflectance was analyzed over different surface types for whole growing seasons. It was found that the BRD depends on wavelength, land cover type, solar zenith angle, and vegetation growing condition. The TOA BRDs generally resemble those obtained from surface measurements of the same type, suggesting the predominant role of the surface BRD in the TOA BRD for the AVHRR measurements over the geographic areas under study. The BRDs for all land cover types investigated here have stronger reflection in the backscattering directions toward the Sun (hot spot). The hot spot effect is more striking in the near-infrared channel than in the visible one. The width and strength of a hot spot are modified

by physical and optical properties of a canopy such as leaf reflectance, transmittance, dimension, plant height and density, etc. Since these properties are related to land cover type and greenness, the effects of canopy physiological condition on BRDF were examined in detail with respect to the changes in NDVI for each land cover type. It was found that the effects are very significant. The seasonal variations of BRD are thus determined by both SZA and NDVI.

The BRDF was therefore developed with four variables, namely, SZA, VZA, RAA, and NDVI for a specific land cover type at each channel. The BRDF is semiempirical, derived from the physically based bidirectional functions proposed by Roujean *et al.* [1992a] with some parameters to be derived empirically from AVHRR measurements. For vegetated cover types considered here, these parameters are given as the functions of NDVI. It was found that a BRDF can produce angular patterns similar to those observed for large ranges of SZA and NDVI over a fixed land cover type. The good agreement between the observed and modeled reflectances suggests that a single BRDF is sufficient to correct the bidirectional dependence in the AVHRR observations for a given land cover type. A BRDF can be used to normalize the reflectance observed at a particular Sun-target-satellite geometry to a reflectance corresponding to a common geometry or to infer an albedo defined over the upper hemisphere. The normalized reflectances exhibit much smoother seasonal variations than the original reflectances, which facilitates statistical analysis and interpretation of AVHRR data for monitoring changes associated with surface conditions.

It should be stated that bidirectional dependency is only one of the problems encountered in the use of AVHRR measurements for detecting changes. Satellite sensor drift, for example, is another important issue in long-term monitoring. This study aims primarily at studying the effects of land cover type and seasonality on the AVHRR bidirectional reflectance distribution. The impacts of the atmosphere and topography are minimized by selecting uniform sites over remote areas. This implies that the BRDF developed in this study may not be applicable to areas of complex topography with strong atmospheric effects due to aerosols and water vapor.

**Acknowledgments.** We thank Joy Hood of the EROS Data Center for providing AVHRR data and relevant information. Constructive comments were made by G. Fedosejevs and G. Gutman. One of the authors, A. Wu, is grateful to the Chinese Academy of Sciences, China, for providing financial support while he visited the CCRS.

## References

- Arking, A., and J. D. Childs, Extraction of cloud cover parameters from multispectral satellite measurements, *J. Clim. Appl. Meteorol.*, **24**, 322–333, 1985.
- Blad, B. L., Measuring and modelling near-surface reflected and emitted radiation, in FIFE April 1988 Workshop Report, pp. 120–129, internal NASA document, International Satellite Land and Surface Climatology Project, Goddard Space Flight Cent., Greenbelt, Md., 1988.
- Cierniewski, J., and D. Courault, Bidirectional reflectance of bare soil surfaces in the visible and near-infrared range, *Remote Sens. Rev.*, **7**, 321–339, 1993.
- Cihlar, J., D. Manak, and N. Voisin, AVHRR bidirectional reflectance effects and composite, *Remote Sens. Environ.*, **48**, 77–88, 1994.
- Coakley, J. A., and F. P. Bretherton, Cloud cover from high-resolution scanner data: Detecting and allowing for partially filled fields of view, *J. Geophys. Res.*, **87**, 4917–4932, 1982.
- Deering, D. W., and E. M. Middleton, Spectral bidirectional reflectance and effects on vegetation indices for a prairie grassland, in *Preprints of the Symposium on FIFE, First ISLSCP Field Experiment*, pp. 71–76, American Meteorological Society, Boston, Mass., 1990.
- D'Iorio, M. A., J. Cihlar, and C. R. Morasse, Effect of calibration of AVHRR data on the normalized difference vegetation index and composite, *Can. J. Remote Sens.*, **3**, 251–262, 1991.
- Gao, W., A simple bidirectional-reflectance model applied to a tallgrass canopy, *Remote Sens. Environ.*, **45**, 209–224, 1993.
- Gerstl, S., and C. Simmer, Radiation physics and modelling for off-nadir satellite-sensing of non-Lambertian surfaces, *Remote Sens. Environ.*, **20**, 1–29, 1986.
- Gutman, G., On the relationship between monthly mean and maximum-value composite normalized vegetation indices, *Int. J. Remote Sens.*, **10**, 1317–1325, 1989.
- Gutman, G., Vegetation indices from AVHRR: An update and future prospects, *Remote Sens. Environ.*, **35**, 121–136, 1991.
- Gutman, G., Normalization of multi-annual global AVHRR reflectance data over land surfaces to common sun-target-sensor geometry, *Adv. Space Res.*, **14**, 121–124, 1994.
- Gutman, G., D. Tarpley, and G. Ohring, Cloud screening for determination of land surface characteristics in a reduced resolution satellite data set, *Int. J. Remote Sens.*, **8**, 859–870, 1987.
- Gutman, G., A. Gruber, D. Tarpley, and R. Taylor, Application of angular models to AVHRR data for determination of the clear-sky planetary albedo over land surfaces, *J. Geophys. Res.*, **94**, 9959–9970, 1989.
- Hapke, B., Bidirectional reflectance spectroscopy, 1, Theory, *J. Geophys. Res.*, **86**, 3039–3054, 1981.
- Holben, B., and R. S. Fraser, Red and near-infrared sensor response to off-nadir viewing, *Int. J. Remote Sens.*, **5**, 145–160, 1984.
- Holben, B., D. S. Kimes, and R. S. Fraser, Directional reflectance response in AVHRR red and near-IR bands for three cover types and varying atmospheric conditions, *Remote Sens. Environ.*, **19**, 213–236, 1986.
- Hood, J. J., Advanced very high resolution radiometer validation data set, paper presented at the 25th International Symposium on Remote Sensing and Global Environmental Change, ERIM/JOANNEUM Res./CIESIN, Graz, Austria, 1993.
- Jupp, D. L. B., and A. H. Strahler, A hotspot model for leaf canopies, *Remote Sens. Environ.*, **38**, 193–210, 1991.
- Kimes, D. S., Dynamics of directional reflectance factor distributions for vegetation canopies, *Appl. Opt.*, **22**, 1364–1372, 1983.
- Kimes, D. S., Modeling the directional reflectance from complete homogeneous vegetation canopies with various leaf-orientation distributions, *J. Opt. Soc. Am.*, **7**, 725–737, 1984.
- Kimes, D. S., and P. J. Sellers, Inferring hemispherical reflectance of the earth's surface for global energy budgets from remotely sensed nadir or directional radiance values, *Remote Sens. Environ.*, **18**, 205–223, 1985.
- Kimes, D. S., B. N. Holben, C. J. Tucker, and W. W. Newcomb, Optimal directional view angles for remote-sensing missions, *Int. J. Remote Sens.*, **5**, 887–908, 1984.
- Kimes, D. S., W. W. Newcomb, R. F. Nelson, and J. B. Schutt, Directional reflectance distributions of a hardwood and pine forest canopy, *IEEE Trans. Geosci. Remote Sens.*, **GE-24**, 281–293, 1986.
- Kriebel, K. T., Measured spectral bidirectional reflection properties of four vegetated surfaces, *Appl. Opt.*, **17**, 253–259, 1978.
- Lee, L., and Y. J. Kaufman, The effect of non-Lambertian surface on remote sensing of surface reflectance and vegetation index, *IEEE Trans. Geosci. Remote Sens.*, **24**, 699–708, 1986.
- Li, X., and A. H. Strahler, Geometric-optical bidirectional reflectance modelling of a conifer forest canopy, *IEEE Trans. Geosci. Remote Sens.*, **GE-24**, 906–919, 1986.
- Li, Z., and L. Garand, Estimation of surface albedo from space: A parameterization for global application, *J. Geophys. Res.*, **99**, 8335–8350, 1994.
- Li, Z., and H. G. Leighton, Global climatology of solar radiation budgets at the surface and in the atmosphere from 5 years of ERBE data, *J. Geophys. Res.*, **98**, 4919–4930, 1993.

- Li, Z., and L. Moreau, A new approach for remote sensing of canopy absorbed photosynthetically active radiation, 1, Total surface absorption, *Remote Sens. Environ.*, in press, 1995.
- Liang, S., and A. H. Strahler, Calculation of the angular radiance distribution for a coupled atmosphere and canopy, *IEEE Trans. Geosci. Remote Sens.*, 31, 491–502, 1993.
- Middleton, E. M., Solar zenith angle effects on vegetation indices in tallgrass prairie, *Remote Sens. Environ.*, 38, 45–62, 1991.
- Mitchell, R. M., and D. M. O'Brien, Correction of AVHRR short-wave channels for the effects of atmospheric scattering and absorption, *Remote Sens. Environ.*, 46, 129–145, 1993.
- Paltridge, G. W., and R. M. Mitchell, Atmospheric and viewing angle correction of vegetation indices and grassland fuel moisture content derived from NOAA/AVHRR, *Remote Sens. Environ.*, 31, 121–135, 1990.
- Pinker, R. T., and L. L. Stowe, Modelling planetary bidirectional reflectance over land, *Int. J. Remote Sens.*, 11, 113–123, 1990.
- Pinty, B., and M. M. Verstraete, On the design and validation of surface bidirectional reflectance and albedo models, *Remote Sens. Environ.*, 41, 155–167, 1992.
- Pinty, B., M. M. Verstraete, and R. E. Dickinson, A physical model for predicting bidirectional reflectances over bare soil, *Remote Sens. Environ.*, 27, 273–288, 1989.
- Rahman, H., M. M. Verstraete, and B. Pinty, Coupled surface-atmosphere reflectance (CSAR) model, 1, Model description and inversion on synthetic data, *J. Geophys. Res.*, 98, 20,779–20,789, 1993.
- Ross, J., and A. L. Marshak, Calculation of the canopy bidirectional reflectance using the Monte-Carlo method, *Remote Sens. Environ.*, 24, 213–225, 1988.
- Roujean, J. L., M. Leroy, A. Leroy, and P. Y. Deschamps, A bidirectional reflectance model of the Earth's surface for the correction of remote sensing data, *J. Geophys. Res.*, 97, 20,455–20,468, 1992a.
- Roujean, J. L., M. Leroy, A. Podaire, and P. Y. Deschamps, Evidence of surface reflectance bidirectional effects from a NOAA/AVHRR multi-temporal data set, *Int. J. Remote Sens.*, 13, 685–698, 1992b.
- Saunders, R. W., An automated scheme for the removal of cloud contamination from AVHRR radiances over western Europe, *Int. J. Remote Sens.*, 7, 867–886, 1986.
- Saunders, R. W., A users guide to the A.P.O.L.L.O., Scheme on HERMES/HOMER, internal report, *Memo.* 87, U.K. Meteorol. Office, Farnborough, Hants, England, 1987.
- Saunders, R. W., and K. T. Kriebel, An improved method for detecting clear sky and cloudy radiances from AVHRR data, *Int. J. Remote Sens.*, 9, 123–150, 1988.
- Sellers, P. J., Canopy reflectance, photosynthesis and transpiration, *Int. J. Remote Sens.*, 8, 1335–1372, 1985.
- Shibayama, M., and C. L. Wiegand, View azimuth and zenith, and solar angle effects on wheat canopy reflectance, *Remote Sens. Environ.*, 18, 91–103, 1985.
- Spanner, M. A., L. L. Pierce, S. W. Running, and D. L. Peterson, The seasonality of AVHRR data of temperate coniferous forests: Relationship with leaf area index, *Remote Sens. Environ.*, 33, 97–112, 1990.
- Strahler, A. H., and D. L. B. Jupp, Geometric-optical modeling of forests as scenes composed of three-dimensional discrete objects, in *Photon-Vegetation Interactions: Applications in Optical Remote Sensing and Plant Ecology*, edited by R. B. Myneni and J. Ross, pp. 415–440, Springer-Verlag, New York, 1990.
- Suttles, J. T., R. N. Green, P. Minnis, G. L. Smith, W. F. Staylor, B. A. Wielicki, I. J. Walker, D. F. Young, V. R. Taylor, and L. L. Stowe, Angular radiation models for Earth-atmosphere system, vol. 1, Shortwave radiation, *NASA Ref. Publ.* 1184, 114 pp., 1988.
- Taylor, V. R., and L. L. Stowe, Reflectance characteristics of uniform Earth and cloud surfaces derived from Nimbus 7 ERB, *J. Geophys. Res.*, 89, 4981–4996, 1984.
- Teillet, P. M., and B. N. Holben, Towards operational radiometric calibration of NOAA AVHRR imagery in the visible and near-infrared channels, *Can. J. Remote Sens.*, 20, 1–10, 1994.
- Verhoef, W., Light scattering by leaf layers with application to canopy reflectance modelling: The SAIL model, *Remote Sens. Environ.*, 16, 125–141, 1984.
- Verstraete, M. M., B. Pinty, and R. E. Dickinson, A physical model of the bidirectional reflectance of vegetation canopies, 1, Theory, *J. Geophys. Res.*, 95, 11,755–11,765, 1990.
- Walthall, C. L., J. M. Norman, J. M. Welles, G. Campbell, and B. L. Blad, Simple equation to approximate the bidirectional reflectance from vegetative canopies and bare soil surfaces, *Appl. Opt.*, 3, 383–387, 1985.

J. Cihlar and Z. Li (corresponding author), Canada Centre for Remote Sensing, 588 Booth, Ottawa, Ontario, Canada, K1A 0Y7.  
A. Wu, Department of Soil Sciences, University of British Columbia, Vancouver, British Columbia, Canada, V6T 1Z4.

(Received September 7, 1994; revised January 21, 1995; accepted February 8, 1995.)